

A Fast Inverse Design Method for Multilayered, Multiport Pixelated Surfaces

Woojun Lee^{#1}, Jungmin Lee^{#2}, and Jeffrey S. Walling^{#3}

[#]MICS and Wireless at Virginia Tech

{¹woojun, ²jmlee22, ³jswalling}@vt.edu

Abstract—This paper presents a fast inverse design framework for complex multilayered, multiport pixelated surfaces – a class of structures largely unexplored in current research. Leveraging a method-of-moments (MoM) electromagnetic (EM) solver, the framework enables the rapid synthesis of pixelated device designs. A novel matrix reconstruction technique, based on pre-labeling matrix entries as "inter-pixel" or "inner-pixel," accelerates simulations for each variation of the pixelated structure. To mitigate the cubic increase in computation time associated with additional layers, GPU acceleration is employed. Further enhancing convergence speed, a stochastic multi-pixel flipping search algorithm is integrated into the framework. The effectiveness of this approach is demonstrated through the design of a diplexer achieving a -3-dB bandwidth for one channel spanning 5.23–5.94 GHz and another covering 6.17–7.15 GHz, validated by a full-wave solver.

Keywords—Inverse design, diplexers, method-of-moment, optimization

I. INTRODUCTION

The increasing demand for compact, high-performance electromagnetic (EM) components has fueled a surge in the development of inverse design algorithms. Traditional inverse design techniques (e.g., genetic algorithms, particle swarm optimization, etc. [1]) offer heuristic approaches to optimize EM structures by systematically exploring their geometric parameters. However, the field has witnessed an increase in more sophisticated techniques. Machine learning-driven EM emulators [2], rapid simulations using finite-difference methods [3], and direct binary search (DBS) algorithms [4] have emerged, pushing the boundaries of design complexity, particularly for intricate structures like pixelated surfaces.

Despite this progress, a significant challenge persists: the inverse design of multi-layered EM devices. Most current algorithms are limited to planar or single-layered geometries, overlooking the potential for compactness and enhanced performance offered by multilayered configurations [5]. This limitation has resulted in a scarcity of research on inverse design methods specifically tailored to multilayered structures.

This paper addresses this gap by introducing a fast inverse design framework based on a search algorithm coupled with a method-of-moments (MoM) solver. This approach tackles two central challenges inherent in multilayered EM device design. First, the computational demands increase dramatically with the addition of layers. Memory requirements grow quadratically due to the expanding matrix size from the increased number of basis functions (BFs). Moreover, computational time for matrix inversion increases cubically

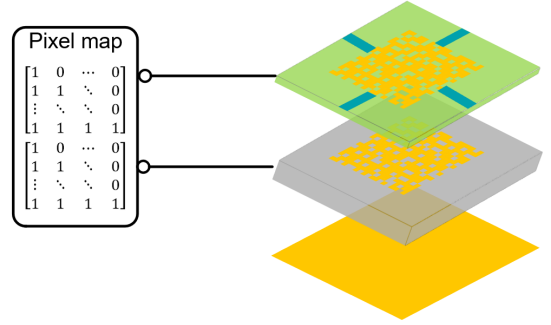


Fig. 1. Multi-layered multi-port inverse design.

with each new layer. Second, achieving an optimal balance between computational speed and accuracy hinges on judicious selection of BFs. An overly fine resolution leads to excessive computational time, while a coarse resolution compromises the accuracy of the results.

II. ALGORITHM

A. Background

One approach to deriving the frequency response of EM devices involves solving the electric field integral equation (EFIE). This method utilizes an equivalent representation of the structure based on the distribution of current density on conducting surfaces. The EFIE is expressed as:

$$\hat{n} \times \vec{E}_{\text{inc}} - \hat{n} \times \iint_S \vec{G}(\vec{r}, \vec{r}') \cdot \vec{J}(\vec{r}') dS' = 0 \quad (1)$$

where \vec{E}_{inc} is the incident electrical field, $\vec{J}(\vec{r}')$ is the surface current density, \hat{n} is the normal vector to the conducting surface, and \vec{G} is the dyadic Green's function, which depends on the dielectric property and configuration of the surfaces.

The Method of Moments (MoM) is a well-established technique for solving the EFIE [6]. By discretizing the conducting surface into smaller meshes and approximating the surface current density using a set of basis functions (BFs), the EFIE is transformed into a matrix equation:

$$ZI = V \quad (2)$$

where Z is an interaction matrix that specifies the relationship between the BF representing the surface current density of the conducting surfaces, V is an excitation vector representing the source, and I is a vector containing the coefficient of each BF to be solved. In this paper, Rao-Wilton-Glisson (RWG) basis

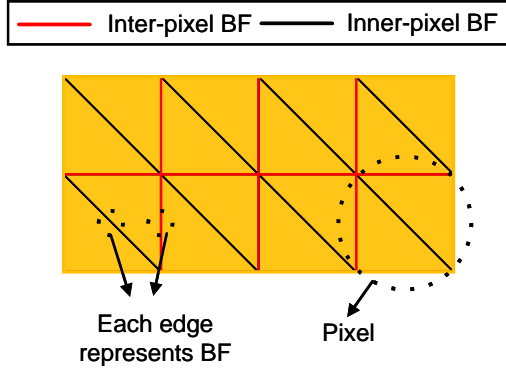


Fig. 2. Classification of basis functions into "inter-pixel," "inner-pixel," and "always-present" categories.

functions are employed [7], where each edge of a triangular mesh defines a BF.

B. Fast Simulation through Matrix Reconstruction

Previous work has explored accelerating the optimization process for pixelated metallic antennas. In [8], a genetic algorithm was used with a technique to construct the impedance matrix (Z) of a sub-structure by selectively removing rows and columns from the original "parent" matrix. A similar approach was employed in [2] to enhance optimization using finite-difference methods.

This paper extends this concept to multi-layered, multi-port metal-dielectric-composite structures. To efficiently reconstruct the Z matrix for different sub-structures, each basis function (BF) is pre-labeled as "inter-pixel," "inner-pixel," or "always-present." "Always-present" BFs represent the current density on the launching section. "Inner-pixel" BFs are activated when their corresponding pixel is "on". "Inter-pixel" BFs are included only when both adjacent pixels are active. This pre-labeling scheme guides the identification of active and inactive BFs during matrix reconstruction. Additional BF classes exist, including those associated with port-pixel intersections, but are not detailed here. This classification process is illustrated in Fig. 2.

To mitigate the cubic increase in computational time associated with matrix inversion for multi-layered structures, graphics processing unit (GPU) acceleration is employed.

C. Stochastic Multi-pixel Flipping Algorithm

To accelerate the inverse design process, a customized version of the direct binary search (DBS) algorithm, referred to as the stochastic multi-pixel flipping algorithm, is employed. This algorithm, outlined in Algorithm 1, iteratively refines a pixel map to optimize a figure-of-merit (FoM). The FoM quantifies the performance of the (EM) device based on the pixel map configuration; its detailed formulation is provided in Section III-A.

The algorithm begins with a random pixel map initialization. It then iteratively updates the map based on the current FoM. Three distinct search strategies are used

Algorithm 1 Optimized Pixelmap Design Algorithm

```

Initialize pixelmap randomly
current_fom  $\leftarrow \infty$ , improvement  $\leftarrow$  False
while True do
  if current_fom > Threshold1 then
    Randomly modify 5 pixels and compute new_fom
  else if Threshold2 < current_fom  $\leq$  Threshold1 then
    Randomly modify 3 pixels and compute new_fom
  else
    for each pixel in pixelmap do
      for valid values of the pixel do
        Compute local_fom for updated pixel
      end for
    end for
  end if
  if new_fom or local_fom improves current_fom then
    Update pixelmap; improvement  $\leftarrow$  True
    Update current_fom
  end if
  if not improvement and current_fom < Threshold2 then
    Break
  end if
end while

```

depending on the FoM. If the FoM exceeds a predefined high threshold (*Threshold1*), five pixels are randomly flipped to explore the design space broadly. When the FoM falls within a medium range (*Threshold2* to *Threshold1*), three pixels are randomly flipped, striking a balance between exploration and refinement. For FoM values below *Threshold2*, an exhaustive search is conducted. Each pixel is systematically evaluated by testing all possible configurations, ensuring a thorough exploration of the local design space.

This adaptive search strategy allows the algorithm to efficiently navigate the design space, balancing exploration and exploitation to converge on an optimal or near-optimal solution. The algorithm terminates when a complete sweep of all pixels results in no further improvement to the FoM.

III. EXAMPLE DESIGN

A. Optimization Setting

To demonstrate the capabilities of the proposed framework, a WiFi 6E diplexer, similar to the one presented in [9], is designed. Two Rogers 4350B substrates are stacked, as depicted in Fig. 3, to create a 4-state pixelated surface. Each pixel can assume one of four states, illustrated in Fig. 4: 0-inactive, 1-top layer active, 2-bottom layer active, or 3-both layers active. These states are represented by unique configurations of red and blue layers, with a dashed outline indicating the pixel boundary.

The geometry and mesh of the "parent" structure, used for generating the initial impedance matrix, are shown in Fig. 5. The width of each port is designed to achieve a 50- Ω impedance. Each pixel is subdivided into eight right triangles. This mesh density was chosen after experimentation: using

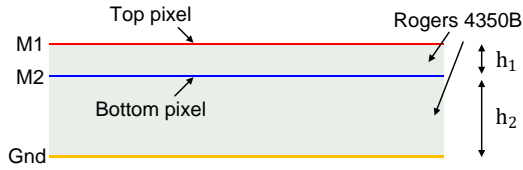


Fig. 3. Dielectric substrate configuration. The substrate material is Rogers 4350B with a dielectric constant of 3.66 and a loss tangent of 0.004. Substrate thicknesses are $h_1 = 0.25\text{mm}$ and $h_2 = 0.76\text{mm}$.

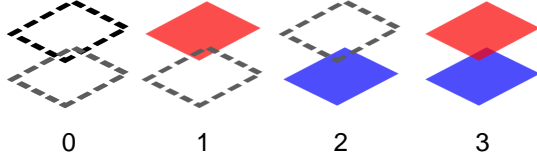


Fig. 4. Possible states for each pixel in the pixel map.

only two triangles per pixel led to significant discrepancies compared to a full-wave solver, while increasing to 16 triangles produced results nearly identical to those obtained with eight. The diagonal orientation of each two-triangle mesh set is randomized to ensure consistent simulation accuracy across different sub-structures.

Port 1 in Fig. 5 is designated as the input port, while ports 2 and 3 serve as output ports for the two diplexer channels. Initial attempts using port 2 as the input often failed to converge to an effective solution. This is likely because achieving the desired asymmetric frequency response is more challenging with a symmetric port configuration.

The figure-of-merit (FoM) function used to guide the optimization process is defined as:

$$\text{FoM} = \sum_{f \in f_1} \frac{1}{rw_1(f)} + \sum_{f \in f_2} \frac{1}{rw_2(f)} + \sum_{f \notin f_1} \frac{1}{rw_3(f)} + \sum_{f \notin f_2} \frac{1}{rw_4(f)} + \sum_{f \in (f_1 \cup f_2)} \frac{1}{rw_5(f)}. \quad (3)$$

where each rewarding function is expressed as:

$$rw_1(f) = 10^{\frac{20 \log_{10} |S_{21}(f)| + 1.0}{10}} \quad (4)$$

$$rw_2(f) = 10^{\frac{20 \log_{10} |S_{31}(f)| + 1.0}{10}} \quad (5)$$

$$rw_3(f) = 10^{\frac{-20 \log_{10} |S_{21}(f)| - 20.0}{15}} \quad (6)$$

$$rw_4(f) = 10^{\frac{-20 \log_{10} |S_{31}(f)| - 20.0}{15}} \quad (7)$$

$$rw_5(f) = 10^{\frac{-10.0 - 20 \log_{10} |S_{11}(f)|}{10}} \quad (8)$$

Each term in the FoM corresponds to a desired passband or stopband response for each channel, with an additional term, $rw_5(f)$, included to ensure good matching at the input port. The target frequency ranges for the two channels are the same as those used in [9]:

$$f_1 = \{f \mid 5.15 \text{ GHz} \leq f \leq 5.925 \text{ GHz}\} \quad (9)$$

$$f_2 = \{f \mid 5.925 \text{ GHz} \leq f \leq 7.125 \text{ GHz}\} \quad (10)$$

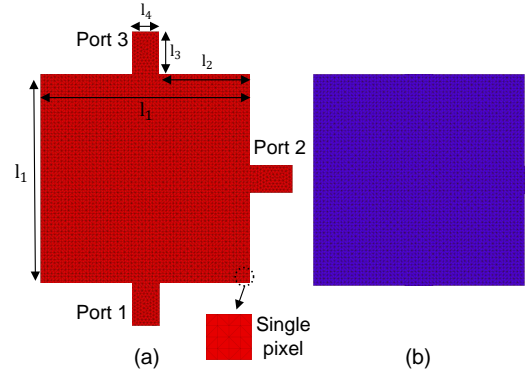


Fig. 5. Geometry and mesh of the parent structure used for generating the initial impedance matrix. (a) Top surface. (b) Bottom surface. Dimensions are $l_1 = 16.764\text{mm}$, $l_2 = 7.2644\text{mm}$, $l_3 = 3.3528\text{mm}$, and $l_4 = 2.2352\text{mm}$.

Table 1. Simulation Parameters

Parameter	Value	Parameter	Value
Pixel dimension	30×30	Threshold1	10000
Pixel size	$0.5588 \text{ mm} \times 0.5588 \text{ mm}$	Threshold2	100
Matrix dimension	22398×22398	No. of frequency points	35

Finally, Table 1 summarizes the key optimization parameters. The 35 frequency points used in the simulation were selected from the following ranges: 23 points linearly spaced in $[5.15\text{GHz}, 7.125\text{GHz}]$, 5 points linearly spaced in $[4.55\text{GHz}, 5.15\text{GHz}]$, 5 points linearly spaced in $[7.125\text{GHz}, 7.725\text{GHz}]$, and two additional frequencies at 4GHz and 8GHz.

B. Results

Fig. 6 presents the results of the inverse design process for multilayered pixelated diplexers. The figure shows three optimized pixel configurations and their corresponding simulated frequency responses. The $(|S_{21}|)$ and $(|S_{31}|)$ responses, obtained using both the MoM solver integrated into the optimization framework and a commercial full-wave HFSS solver, demonstrate good agreement. It is noted that both simulations were conducted with pixel sets configured such that pixels intersecting at a single point are treated as disconnected.

While the results validate the effectiveness of the proposed inverse design approach, a minor rightward frequency shift is observed between the MoM and HFSS results, indicating an area for potential refinement in the future. The configuration shown in Fig. 6(a) exhibits the best performance, achieving a -3 dB bandwidth of 5.23-5.94 GHz for $(|S_{21}|)$ and 6.17-7.15 GHz for $(|S_{31}|)$.

Although the stopband rejection performance of the designed diplexers does not yet match that of the diplexer presented in [9], several strategies can be explored to further enhance the design. Incorporating a double-grounded structure could improve the quality factor of the bandstop resonance by minimizing radiation losses. Additionally, varying the overall dimensions of the top and bottom pixel maps could

REFERENCES

- [1] D. W. Boeringer and D. H. Werner, "Particle swarm optimization versus genetic algorithms for phased array synthesis," *IEEE Transactions on antennas and propagation*, vol. 52, no. 3, pp. 771–779, 2004.
- [2] Y. Zheng and C. Sideris, "Ultra-fast simulation and inverse design of metallic antennas," in *2023 IEEE/MTT-S International Microwave Symposium-IMS 2023*. IEEE, 2023, pp. 351–354.
- [3] E. A. Karahan, Z. Liu, and K. Sengupta, "Ims deep learning enabled generalized synthesis of multi-port electromagnetic structures and circuits for mmwave power amplifiers," in *2024 IEEE/MTT-S International Microwave Symposium-IMS 2024*. IEEE, 2024, pp. 184–187.
- [4] J. Lee, W. Jia, B. Sensale-Rodriguez, and J. S. Walling, "Pixelated rf: Random metasurface based electromagnetic filters," in *2023 21st IEEE Interregional NEWCAS Conference (NEWCAS)*. IEEE, 2023, pp. 1–5.
- [5] A. Belenguier, M. D. Fernandez, J. A. Ballesteros, J. J. de Dios, H. Esteban, and V. E. Boria, "Compact multilayer filter in empty substrate integrated waveguide with transmission zeros," *IEEE Transactions on Microwave Theory and Techniques*, vol. 66, no. 6, pp. 2993–3000, 2018.
- [6] R. F. Harrington, "The method of moments in electromagnetics," *Journal of Electromagnetic waves and Applications*, vol. 1, no. 3, pp. 181–200, 1987.
- [7] S. Rao, D. Wilton, and A. Glisson, "Electromagnetic scattering by surfaces of arbitrary shape," *IEEE Transactions on antennas and propagation*, vol. 30, no. 3, pp. 409–418, 1982.
- [8] J. M. Johnson and Y. Rahmat-Samii, "Genetic algorithms and method of moments (ga/mom) for the design of integrated antennas," *IEEE Transactions on Antennas and Propagation*, vol. 47, no. 10, pp. 1606–1614, 1999.
- [9] S. Gupta, E. Mehdizadeh, K. Cheema, and J. Shealy, "Miniaturized ultrawide bandwidth wifi 6e diplexer implementation using xbow rf filter technology," in *2022 IEEE/MTT-S International Microwave Symposium-IMS 2022*. IEEE, 2022, pp. 880–882.

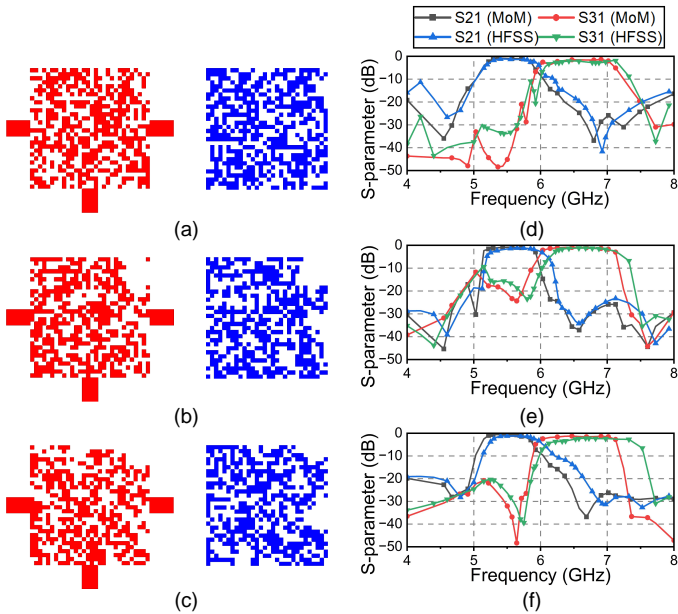


Fig. 6. Inversely designed multilayered pixelated diplexers and their simulated frequency responses. (a)-(c) Optimized pixel configurations, where red represents active pixels in the top layer and blue represents active pixels in the bottom layer. (d)-(f) Corresponding ($|S_{21}|$) and ($|S_{31}|$) responses obtained from both MoM and HFSS simulations.

be investigated, as the frequency response of the diplexer is significantly influenced by these dimensions.

The computational cost of the optimization process is summarized as follows. Simulating the 35 parent matrices required ≈ 8 hours using 12 Intel Xeon E5-2620 CPUs (144 cores). Each iteration of the optimization algorithm took approximately 13 seconds, resulting in a total optimization time of ≈ 8 hours. This phase was conducted on a 32-core AMD EPYC 7742 CPU, with matrix inversion tasks offloaded to two 80 GB NVIDIA A100 GPUs. It is worth noting that matrix inversion dominated the overall optimization time, highlighting the effectiveness of the GPU acceleration in this process.

IV. CONCLUSION

This paper presented a fast inverse design framework for multilayered, multiport pixelated surfaces. The framework utilizes a search optimization algorithm based on pre-computed matrices, coupled with a stochastic multipixel flipping algorithm and GPU acceleration. This methodology enables rapid evaluation and optimization of multilayered device configurations, completing the entire process within a single day. The accuracy of the method was verified through full-wave simulations. The results demonstrate the potential of EM multilayered filters and diplexers as cost-effective alternatives to their acoustic-wave-based counterparts. Futures work include the design and experimental fabrication of more complex multilayered structures incorporating vertical vias.